University of Nebraska - Lincoln
DigitalCommons@University of Nebraska - Lincoln

Christian Binek Publications | Research Papers in Physics and Astronomy

4-7-2009

Magnetocaloric properties of Co/Cr superlattices

Tathagata Mukherjee
University of Nebraska at Lincoln, tathagata.mukherjee@huskers.unl.edu

Sarbeswar Sahoo
University of Nebraska-Lincoln, ssahoo2@unlnotes.unl.edu

David J. Sellmyer
University of Nebraska at Lincoln, dsellmyer@unl.edu

Christian Binek
University of Nebraska, Lincoln, cbinek2@unl.edu

Follow this and additional works at: http://digitalcommons.unl.edu/physicsbinek

Part of the Physics Commons

Mukherjee, Tathagata; Sahoo, Sarbeswar; Sellmyer, David J.; and Binek, Christian, "Magnetocaloric properties of Co/Cr superlattices" (2009). *Christian Binek Publications.* Paper 66.
http://digitalcommons.unl.edu/physicsbinek/66

This Article is brought to you for free and open access by the Research Papers in Physics and Astronomy at DigitalCommons@University of Nebraska - Lincoln. It has been accepted for inclusion in Christian Binek Publications by an authorized administrator of DigitalCommons@University of Nebraska - Lincoln.

Magnetocaloric properties of Co/Cr superlattices

T. Mukherjee, S. Sahoo, R. Skomski, D. J. Sellmyer, and Ch. Binek*
Department of Physics and Astronomy and the Nebraska Center for Materials and Nanoscience, University of Nebraska, Lincoln, Nebraska 68588-0111, USA

(Received 20 December 2008; revised manuscript received 6 March 2009; published 7 April 2009)

Nanostructured materials for refrigeration applications are experimentally realized by molecular beam epitaxial growth of Co/Cr superlattices using mean-field theoretical concepts as guiding principles. Magnetocaloric properties are deduced from measurements of the temperature and field dependence of the magnetization of our samples. More generally, the potential of artificial antiferromagnets for near room-temperature refrigeration is explored. The effects of intraplane and interplane exchange interactions on the magnetic phase diagram in Ising-type model systems are revisited in mean-field considerations with special emphasis on tailoring magnetocaloric properties. The experimental results are discussed in light of our theoretical findings, and extrapolations for future improved nanostructures are provided.

DOI: 10.1103/PhysRevB.79.144406 PACS number(s): 75.30.Sg, 75.30.Kz, 75.70.Cn

I. INTRODUCTION

Magnetic refrigeration is expected to play an important role in the quest for energy-efficient and environmentally friendly technologies of the near future.[1–4] The magnetocaloric effect (MCE) provides the physical basis of magnetic refrigeration technology which has the potential to replace today's common compression refrigerators.[5–8] The temperature change induced in a magnetic material during an adiabatic magnetic field change and the change in the isothermal magnetic entropy are two of the most important parameters that characterize and quantify the MCE.[9] A straightforward path to enhance the field-induced entropy change is realized when isothermally increasing the applied magnetic field until technical saturation of the magnetization is reached. This brute-force approach has practical limitations. When relying on the maximum achievable flux densities of 1–2 T of modern permanent magnets[10,11] such as Nd-Fe-B and Sm-Co the feasible adiabatic temperature changes still remain below 10 K.[12,13] Permanent magnetic fields of the order of 4 T can be created in Halbach cylinders, but the logarithmic dependence of the created field on the diameter of the cylinder makes such devices very heavy.[11]

To achieve an appreciable MCE with moderate applied magnetic fields new magnetic materials with tailored magnetocaloric properties must be synthesized. This quest pushes the technological frontiers and is cutting-edge materials science.[14–17] Only significant advances in materials science allow systematic progress in magnetic cooling technology and therefore a world-wide search for magnetocaloric materials with high relative cooling power is taking place. These significant efforts are triggered to a large extent by the potential applications such as household refrigerators, cooled infrared charge-coupled device (CCD) cameras, air conditioning in all-electric cars, and portable refrigerators. However, the challenges for the materials scientists are complex. First one must find cost effective, stable, and environmentally friendly materials that maximize the MCE in the vicinity of room temperature while the temperature of peak performance should be tunable in a wide range between the high- and low-temperature baths to optimize cyclic operating cooling devices.[1] Second, one must tailor the dynamic properties involved in the magnetization relaxation process for applications in refrigeration technology.[18,19] This is a particular issue when structural phase transitions contribute to the entropy change, as they do in the recently discovered giant MCE.[14] In fact, the capability of fast demagnetization of a magnetocaloric material is essential when high operation frequency is envisioned which in turn is crucial to take advantage of the proportionality between operation frequency and cooling power.[1,19]

Despite the challenges originating from the dynamic properties of materials, most of today's research activities focus on the giant MCE in bulk materials such as $Gd_3Ge_2Si_2$ (Refs. 20 and 13) and related Gd alloys.[21] Recently, materials undergoing metamagnetic transitions generated interest as potential materials with appreciable MCE.[22–27] This includes low-spin to high-spin transitions, transitions from antiferromagnetic (AF) to ferromagnetic (FM) order, and field-induced magnetization states. The AF to FM transition has the advantage over FM to paramagnetic (PM) transitions that the applied magnetic fields necessary for magnetic entropy changes do not destroy and, hence, smear out the criticality of the phase transition. Steepness of the temperature dependence of the magnetization in a large magnetic field range is the key for large entropy changes and adiabatic temperature changes. Some bulk materials which involve metamagnetic transitions of interest are Ho_5Pd_2, $Nd_{0.5}Sr_{0.5}MnO_3$, and $Fe_{0.8}Mn_{1.5}As$ to name just a few exotic examples.

Past research has focused on conventionally processed bulk alloys, which can be produced in large quantities, but the range of suitable compounds is limited. Furthermore, many major constituents in MCE alloys, such as Gd, are expensive, their availability in large quantities is limited and often they are objectionable from an environmental point of view.

Virtually unexplored scientific terrain is the nanotechnological approach in magnetocaloric materials design. In this paper we outline our efforts toward new nanostructured materials with a tailored MCE. In order to avoid any misconception about the approach we advocate in this paper, we do not propose to replace magnetocaloric bulk systems by simple superparamagnetic nanoparticles. In the former the entropy changes are realized via spin rearrangements on the atomic scale while the majority of the spin degrees of freedom in the superparamagnetic nanoparticles is frozen and do

 ©2009 The American Physical Society

not contribute to the entropy change.[28] For this reason, simple noninteracting superparamagnetic nanoparticles can hardly be of any advantage. Our aim is to widen the range of materials suitable for magnetic cooling by tailoring interactions in and between ultrathin films or particles. Using simple magnetic materials and realizing the design of the macroscopic properties via nanostructuring provides a huge opportunity to harness the full potential of the MCE.

Nanotechnology allows overcoming some of the limitations of the traditional bulk processing approaches where the flexibility of tailoring microscopic parameters is widely constrained for instance by equilibrium thermodynamics of compositional phase diagrams. Hence, tailoring of macroscopic magnetic properties is limited. Controlled growth of magnetic multilayer structures of ultrathin constituents opens the possibility to exploit the microscopic parameter space in a systematic manner.[29] Here we demonstrate the tailoring of magnetic properties such as the critical temperature of ferromagnetic constituent films by geometrical confinement and interaction between the latter via nonmagnetic spacer layers of controlled thickness. In multilayers of ultrathin films, it is possible to exploit individual microscopic spin degrees of freedom, because spin fluctuations at magnetic phase transitions in reduced dimensions yield a pronounced entropy change. In this sense it is possible to harness the advantages of the bulk and the nanomagnetic world where large spin fluctuations are thermally activated using coupled two-dimensional (2D) subsystems with controlled strength and sign of the magnetic interactions.

In this paper, we discuss the concept of magnetic cooling using multilayers, provide an experimental proof of principle, and explain the involved thermodynamics by a two-sublattice mean-field model.

II. CONCEPT OF SUPERLATTICES FOR MAGNETOCALORIC APPLICATIONS

Conceptually we suggest the following means to achieve a high MCE in nanostructured multilayers in the vicinity of room temperature:

(i) Growth of ultrathin FM films such that finite-size scaling effects allow one to tailor the Curie temperature of the films and the crossover to reduced spatial dimension enhances spin fluctuations.[30–32]

(ii) AF interlayer coupling of the FM constituent films allowing one to tailor a metamagnetic transition with pronounced temperature dependence of the transition line and a prominent magnetic discontinuity at the transition.[33–36]

(iii) Adjusting the FM to PM transitions of the FM constituent films with the global metamagnetic transition for maximum entropy change.

We use molecular beam epitaxial (MBE) growth to tailor the figure of merit of nanostructured magnetocaloric materials.[1] The flaw of limited material production by MBE methods below the scale of a few grams required for refrigeration applications is partially compensated by three aspects. First, at this stage we are concerned with a proof of principle showing the possibility of new nanostructured magnetocaloric materials. Second, we envision a variety of applications where miniaturization is crucial and energy-efficient cooling is required only for small objects with low total heat capacity. Third, one can envision alternative production schemes once an optimized magnetic nanostructure has been demonstrated.

The experimental work is accompanied and guided by theoretical analysis. In this paper, we introduce mean-field considerations that show the path toward optimized thin-film superlattices and report on our experimental results on Co/Cr multilayer systems as an example of this approach. We demonstrate that tailoring of the exchange interaction between the Co layers through subnanometer thickness control of the Cr films together with adjusting of the critical temperature of each individual Co layer through geometrical confinement allows the tuning of the macroscopic magnetization properties. From the temperature dependence of the magnetization in the presence of various applied fields we derive the isothermal entropy change. For magnetization data obtained in a homogeneous phase we use Maxwell's relation and estimate the adiabatic temperature change. Based on our finding we outline a path toward future improved nanostructured magnetocaloric materials.

III. STRUCTURE AND MAGNETISM OF SUPERLATTICES FOR MAGNETOCALORIC APPLICATIONS

A. Multilayer approach for negative MCE

Our multilayer growth follows two major strategies, both aiming at the realization of artificial AF multilayer structures with tailored transition temperatures and maximized isothermal entropy changes. The basic mean-field considerations are not system specific. For simplicity we restrict ourselves to Ising systems despite the fact that our experimental systems have no pronounced uniaxial anisotropy. Hence, the theoretical results can only be considered as conceptual guiding principles. Furthermore, our exclusive magnetic consideration does not take into account potential structural phase transitions which often accompany the magnetic first-order transition and can give rise to significant entropy contributions beyond the magnetic limit $\Delta S_{\max} = Nk_B \ln 2$ or $Nk_B \ln(2S+1)$ for non-Ising systems.[37]

Our experimental investigations presented here focus on Co/Cr superlattices. This system allows the tailoring of the intra- and interlayer magnetic properties entering the theory. In our Co/Cr multilayers, we exploit the fact that the Curie temperature of the FM Co constituents can be tailored in thin films through thickness variation.[31,32] While lowering the Curie temperature from its bulk value of $T_C^{\text{bulk}}(\text{Co}) = 1388$ K to room temperature a dimensional crossover from three-dimensional (3D) to 2D takes place which enhances the spin fluctuations and their contribution to the magnetic entropy.[38]

On the other hand, Cr is a prototypical spacer material for the realization of AF interlayer coupling. The AF coupling strength is an oscillating function of the Cr thickness and can be experimentally tailored.[39–41] Moreover, the spins of the Cr interlayer films support the MCE beyond their task in providing the RKKY-type coupling between the Co films. Note that at thicknesses below 20 monolayers the Cr films are

PM,[40] whereas bulk Cr orders antiferromagnetically with an incommensurate spin-density wave.[40,42] Temperature driven AF transitions have two regions which show a potentially large MCE. On the most interesting low-temperature side the temperature derivative $\partial M/\partial T>0$ of the magnetization, M, maximizes close to the transition temperature where the AF order parameter approaches zero. This is the region of negative MCE which is defined by an adiabatic temperature change smaller than zero when a positive magnetic field is applied. Ultimately we are aiming at an AF-to-PM transition close to the temperature where the FM-to-PM transition of the 2D FM constituent films takes place. The 3D nature of the global AF transition will allow for an optimized MCE. This intuitive picture will be subsequently quantified in a mean-field analysis.

In particular in simple layered structures the AF transition can be transformed into a first-order metamagnetic transition via the ratio of the intralayer and interlayer exchange.[43–46] For a magnetic transition of first order the entropy change at the transition is given by the Clausius-Claperyon equation,

$$\Delta S = -\mu_0 V \frac{dH_m}{dT}\Delta M, \tag{1}$$

where V is the sample volume and dH_m/dT is the slope of the first-order phase-transition line. In a metamagnetic antiferromagnet the latter is separated from the critical line, $H_c(T)$, via a tricritical point.[43] The slope, dH_m/dT, of the first-order transition line and the magnetization discontinuity, ΔM, at the transition are determined by the microscopic exchange parameters and by the atomic coordination. Note that additional field-induced entropy changes take place below and above the transition and can be calculated from the Maxwell relation subject to homogeneity and equilibrium conditions.

Ising metamagnets are modeled by the Hamiltonian,

$$\hat{H} = -\sum_{i,j} J_{ij}\sigma_i\sigma_j - \mu\mu_0 H\sum_i \sigma_i, \tag{2}$$

where $\sigma_i = \pm 1$ are classical Ising variables, μ is the magnitude of the magnetic spin moment, and J_{ij} describes the exchange interaction between the ith and jth atom while the (i,j) summation runs over nearest- and next-nearest-neighbor spins. Griffiths[47] and many others used Ising and Heisenberg localized spin Hamiltonians to investigate the thermodynamics of model systems with competing AF and FM interactions with special emphasis, however, on the critical behavior. The magnetocaloric behavior of the Co/Cr superlattices is a nanoscale effect and generally involves many nonequivalent crystallographic sites (sublattices), but the involved thermodynamics can already be seen from a relatively simple two-sublattice model with competing intra- and intersublattice interactions. Here we use J_1 for the FM interaction in the Co layers and J_2 for the AF exchange mediated by the Cr layer. By analyzing the metamagnetic phase diagrams of Ising antiferromagnets in the mean-field approximation it can be shown that the slope dH_m/dT of the first-order transition line can be tailored by the ratio $\varepsilon = z_1|J_1|/(z_2|J_2|)$, where the coordination numbers $z_{1,2}$ are the only relevant properties of the lattice structure within mean-field approximation.[44] It is this dependence of dH_m/dT and ΔM on the exchange constants and coordination numbers which guides the growth of our magnetic thin-film heterostructures with large MCE.

Using $J_{+/-} := z_1|J_1| \pm z_2|J_2|$ one obtains the slope of the critical line from differentiation of[42]

$$\frac{\mu_0 V M_s}{J_+} H_c(T) = -\frac{\varepsilon - 1}{\varepsilon + 1}\sqrt{1 - T/T_N} + \frac{T}{2T_N}\ln\frac{1 + \sqrt{1 - T/T_N}}{1 - \sqrt{1 - T/T_N}}, \tag{3}$$

where $T_N = \frac{J_+}{k_B}$. At the tricritical temperature $T_{\text{tri}} = T_N(1 - \frac{1}{3\varepsilon})$ the slope reads as[42,43]

$$\frac{\mu_0 V M_s T_N}{J_+}\left.\frac{dH_C}{dT}\right|_{T=T_{\text{tri}}} = \frac{1}{2}\ln\frac{\sqrt{3\varepsilon} + 1}{\sqrt{3\varepsilon} - 1} - \frac{\sqrt{3\varepsilon}}{(\varepsilon + 1)}, \tag{4}$$

At $T < T_{\text{tri}}$ but close to the tricritical temperature one obtains $\frac{dH_m}{dT}|_{T\approx T_{\text{tri}}} \approx \frac{dH_C}{dT}|_{T=T_{\text{tri}}}$. Far below the tricritical temperature the spin-flip field, H_m, is determined by the exchange energies which an applied field has to overcome in order to flip the system from an AF into an almost saturated magnetization state. The metamagnetic transition is then virtually temperature independent, and $\frac{dH_m}{dT}|_{T\to 0} \to 0$. In first approximation we can linearly interpolate between the $T=0$ and $T=T_{\text{tri}}$ behavior obtaining

$$\frac{dH_m}{dT} \approx \frac{T}{T_{\text{tri}}}\left.\frac{dH_C}{dT}\right|_{T=T_{\text{tri}}}, \tag{5}$$

which is used as input for the evaluation of the entropy change at the transition with the help of Eq. (1).

Next we derive an expression for the field-induced magnetization change ΔM at the metamagnetic transition. While $\frac{dH_m}{dT}$ maximizes on approaching the tricritical point ΔM goes to zero because the first-order transition crosses over into critical behavior.[43] At $T \to 0$ the field-induced metamagnetic transition drives the system from zero magnetization to saturation magnetization, M_S, yielding $\Delta M(T=0) = M_s$. Below, we suggest an interpolating expression for the ε and T dependence of ΔM. Armed with this expression, we will be able to quantitatively analyze Eq. (1) and predict the exchange ratio ε that maximizes the entropy change in the vicinity of room temperature.

Kincaid and Cohen[43] studied metamagnetic phase diagrams in the mean-field approximation. Others later continued their work.[44] In mean-field approximation, an Ising Hamiltonian of the type of Eq. (2) with FM intrasublattice and AF intersublattice interactions gives rise to two coupled equations for the two sublattice magnetizations M_A and M_B which read

$$\frac{M_A}{M_s} = (\varepsilon + 1)\left(\frac{\mu_0 V M_s H}{J_+} + \frac{\varepsilon}{\varepsilon + 1}\frac{M_B}{M_s} - \frac{T}{2T_N}\ln\frac{1 + M_B/M_s}{1 - M_B/M_s}\right), \tag{6a}$$

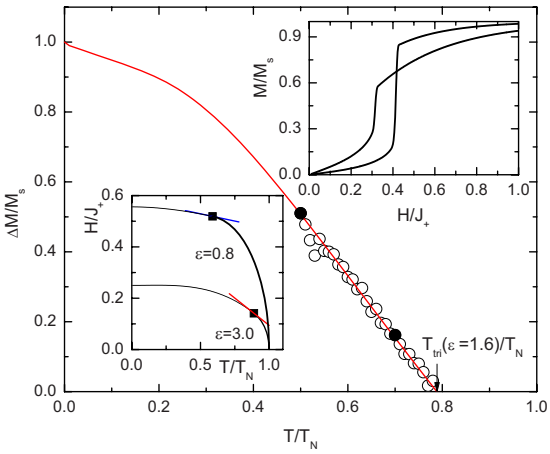

FIG. 1. (Color online) Temperature dependence $\Delta M(T)/M_s$ for $\varepsilon=1.6$ (open circles) obtained from the magnetization jumps in the numerically calculated isotherms $M(H)/M_s$. The upper right inset shows two isotherms for $\varepsilon=1.6$ at $T/T_N=0.5$ and 0.7. Their $\Delta M/M_S$ values are highlighted as solid circles in the main frame. The line represents the parameter free function Eq. (7) and is not a fit. The lower left inset shows the magnetic phase diagram for $\varepsilon=0.8$ and $\varepsilon=3.0$, respectively. The solid curves represent the second-order phase transitions. At the tricritical point (squares) the second-order transition changes into a first-order transition (dotted line). The slope of the transition line at the tricritical point is visualized by tangents (solid lines).

$$\frac{M_B}{M_s}=(\varepsilon+1)\left(\frac{\mu_0 V M_s H}{J_+}+\frac{\varepsilon}{\varepsilon+1}\frac{M_A}{M_s}-\frac{T}{2T_N}\ln\frac{1+M_A/M_s}{1-M_A/M_s}\right). \tag{6b}$$

Analysis of Eqs. (6a) and (6b) shows that a tricritical point emerges for $\varepsilon>3/5$.[42] The asymptotic behavior of $\Delta M=(M_A+M_B)/2$ has been derived for $T\to 0$ and $T\to T_{\text{tri}}$ and reads[43]

$$\Delta M(T)/M_s = 1-3e^{-2\varepsilon T_N/[(\varepsilon+1)T]} \quad \text{for} \quad T\to 0, \tag{7}$$

$$\Delta M(T)/M_s \propto (T-T_{\text{tri}}) \quad \text{for} \quad T\to T_{\text{tri}}. \tag{8}$$

The analytic expression

$$\Delta M(T)/M_s = 3\{e^{-2\varepsilon T_N/[(\varepsilon+1)T_{\text{tri}}]}-e^{-2\varepsilon T_N/[(\varepsilon+1)T]}\} + \{3e^{-2\varepsilon T_N/[(\varepsilon+1)T_{\text{tri}}]}-1\}(T-T_{\text{tri}})/T_{\text{tri}} \tag{9}$$

reproduces the two analytically derived[43] asymptotic expressions (7) and (8) and provides a parameter free fit of the numerically calculated data for $\Delta M(T)/M_s$.

Figure 1 shows our numerical results $\Delta M(T)/M_s$ for $\varepsilon=1.6$ (open circles). They have been obtained from the magnetization discontinuities in the isotherms M/M_s vs H, as calculated from the numerical solutions of the coupled Eqs. (6a) and (6b). The upper right inset shows two typical isotherms for $\varepsilon=1.6$ at $T/T_N=0.5$ and 0.7. The $\Delta M/M_s$ values corresponding to these isotherms are highlighted in Fig. 1 as solid circles. The line representing the parameter free function given by Eq. (9) is not a fit. The lower left inset shows the magnetic phase diagram for $\varepsilon=0.8$ and $\varepsilon=3.0$, respectively. The solid curves represent the second-order phase transitions. At the tricritical point (squares) the second-order transition changes into a first-order transition (dotted line). The slope of the transition line at the tricritical point is visualized by tangents (solid lines). The lower left inset of Fig. 1 shows the magnetic phase diagram for $\varepsilon=0.8$ and $\varepsilon=3.0$, respectively. The solid curves represent the second-order phase transitions. At the tricritical point (squares) the second-order transition changes into a first-order transition (dotted line). The slope of the transition line at the tricritical point is visualized by tangents (solid lines). Inspection of these phase diagrams demonstrates the mechanism of tailoring the isothermal entropy change. At temperatures $T\ll T_{\text{tri}}$ the magnetization discontinuity is very large, however, $dH_c/dT\approx 0$. At the tricritical point dH_c/dT is nonzero and can be tuned via ε, however, the magnetization discontinuity goes to zero on approaching T_{tri}. The optimization of this competition reflects the optimization of the MCE.

Combining the results of Eqs. (4), (5), and (9), and their substitution into Eq. (1) allows to look for the maximum of $|\Delta S(T,\varepsilon)|$ as a function of T and ε. From

$$d|\Delta S(T,\varepsilon)|/dT=0 \quad \text{and} \quad d|\Delta S(T,\varepsilon)|/d\varepsilon=0, \tag{10}$$

we obtain a condition for the optimized ε and a condition for the temperature T^* which defines the optimized operating temperature of the refrigerator. For many applications, including household refrigeration applications T^* must be in the vicinity of room temperature.

Analysis of Eq. (10) yields $T^*\approx 0.53\ T_{\text{tri}}$ and $\varepsilon=2.9$ which in summary means $T_{\text{tri}}\approx T_N\approx 2T^*$. Choosing $T^*\approx 300$ K for near room-temperature refrigeration applications yields $T_{\text{tri}}\approx 600$ K and corresponds to an optimized $T_N\approx 600$ K. Simultaneously satisfying the condition of a high Néel temperature and of a large ε requires weak AF coupling such that T_N is completely dominated by the FM in-plane interaction in accordance with

$$T_N := T_N(H=0)=\frac{J_+}{k_B}. \tag{11}$$

The weak but finite AF coupling guarantees a crossover into 3D AF long-range order despite the strong FM interaction in the Co planes. Physically, the entropy associated with this transition originates from spins that are correlated predominantly in individual layers, with much less pronounced interlayer correlations. A crossover such as this from 2D FM to 3D AF long-range order is well known from the atomic metamagnets such as the prototypical system $FeCl_2$.[45,48–51] The FM intraplane interaction determines the T_C of the individual Co planes and gives rise to the final optimized sample properties $T_{\text{tri}}\approx T_N\approx T_C\approx 2T^*$.

Note that the previous considerations are based on mean-field theory. This reflects our intuitive ideas (i)–(iii) stating that a system with an ideally tailored MCE should take advantage of a first-order transition below room temperature while the proximity of the in-plane T_C and the T_N of the 3D transition thermally activates microscopic spin fluctuations. Hence in contrast to other nanoparticle based magnetocaloric

systems our structures activate the microscopic spin degrees of freedom for contributions to the overall field-induced entropy change.

B. Multilayer approach for positive MCE

Above the AF transition temperature and in moderate magnetic fields, the magnetization follows the functional form,

$$M = \chi(T,\theta)H, \tag{12}$$

where $\chi(T,\theta)=C/(T-\theta)$ is the Curie-Weiss type susceptibility with Curie constant $C>0$ and Curie Weiss temperature $\theta(H=0)=\frac{J_-}{k_B}<T_N(H=0)=\frac{J_+}{k_B}$.[43,44] Often but not necessarily $\theta<0$ is realized in the case of strong AF exchange and high coordination.[46] Here we are interested in realizing systems with $\theta>0$ for enhanced susceptibility. As a general result we obtain $\frac{\partial M}{\partial T}=\frac{-CH}{(T-\theta)^2}<0$ in positive applied magnetic fields. This is the region of positive MCE which is defined by an adiabatic temperature change larger than zero when a positive magnetic field is applied. This behavior of $\partial M/\partial T$ is at first sight very similar to ferromagnets above their Curie temperature. However, one of the major advantages of antiferromagnets over FM systems is the fact that in lowest-order approximation the applied magnetic field does not perturb the AF criticality. A moderate homogeneous magnetic field is an irrelevant field meaning not conjugate to the AF order parameter. As a consequence, criticality is not destroyed by moderate fields H and the shift of the critical temperature $T_N(H)$ and the Curie-Weiss temperature $\theta(H)$ are negligible evolving from $T_N(H=0)$. This is because $(dT_N/dH)_{H=0}=0$ according to $T_N(H)=T_N-\delta|H|^\gamma$, where $\delta>0$ is a small parameter and $\gamma=2$ for 3D Ising antiferromagnets for instance.[52]

Similar to the arguments which lead to the optimization of the metamagnetic transition at $T^*\approx 0.53\ T_{\text{tri}}$ and to negative MCE, tuning of the interaction can shift the temperature and magnetic field ranges to realize appreciable entropy changes with positive MCE in the technically relevant temperature range.

Quantitative benefits of this approach become more transparent when considering the Landau theory for a ferromagnet and its isothermal entropy changes. Above T_N the FM nature of the Co layers dominates the spin-fluctuation spectrum and the Landau expansion of the free-energy density in powers of the FM order parameter M becomes a meaningful description. It reads as

$$F/\mu_0 V = \frac{1}{2}a_0(T-T_C)M^2 + \frac{1}{4}bM^4 - MH, \tag{13}$$

with sample volume V, critical temperature T_C and a_0, $b>0$. From the equilibrium condition $\partial F/\partial M=0$ one obtains the well-known equation of state,

$$a_0(T-T_C)M + bM^3 = H, \tag{14}$$

allowing to derive the expression,

$$\frac{\partial M}{\partial T} = -a_0 M\chi \tag{15}$$

via implicit differentiation with respect to T and H. Here $\chi=\frac{\partial M}{\partial H}=\frac{1}{a_0(T-T_C)+3bM^2}$ is the FM susceptibility in a field. Equation (15) is a compact and generalized expression of corresponding results obtain from more involved mean-field considerations.[53] In particular at $T=T_C$ Eq. (14) yields $M(T=T_C,H)=(H/b)^{1/3}$ which leads to $\frac{\partial M}{\partial T}|_{T=T_C}=-\frac{a_0}{3b}(\frac{b}{H})^{1/3}$. Using Maxwell's relation,

$$\Delta S_m = \mu_0 V\int_{\mu_0 H_i}^{\mu_0 H_f}\frac{\partial M}{\partial T}dH, \tag{16}$$

for the isothermal entropy change induced by a field increase from the initial value, H_i, to the final value, H_f, one obtains the well-known functional form,

$$\Delta S_m/\mu_0 V = -\frac{a_0}{2}\left(\frac{H_f-H_i}{b}\right)^{2/3}. \tag{17}$$

This equation has been verified for various ferromagnets such as the prototypical Gd for instance.[53]

In addition to the alternative derivation of the entropy change, Eq. (15) provides a useful insight into the possibilities to increase the positive MCE. The major limiting factor of the positive MCE is the decay of χ with increasing field or magnetization, which reflects the loss of criticality in the presence of the conjugate field H. This fast decay of χ overcompensates the explicit linear increase in $|\partial M/\partial T|$ with increasing M. An antiferromagnet at $T>T_N$ but not too far above the Curie-Weiss temperature can show appreciable field-induced magnetization while at the same time χ remains virtually unchanged resulting in a potentially large positive MCE. Our approach of nanostructured materials resembles these basic ideas.

C. MBE growth of Co/Cr superlattices

The multilayer systems Cr(10 nm)/[Co(d_{Co})/Cr(0.75 nm)]$_{20}$/Cr(2 nm) with d_{Co}=0.35 and 0.58 nm, Cr(10 nm)/[Co(0.6 nm)/Cr(0.78 nm)]$_{20}$/Cr(2 nm) and Cr(10 nm)/[Co(0.7 nm)/Cr(0.84 nm)]$_{20}$/Cr(2 nm) were prepared by MBE at a chamber base pressure of 1×10^{-10} mbar. The (110)-oriented MgO substrate was heated for 30 min at a temperature of 1023 K in ultrahigh vacuum for degassing and cleaning the surface. The substrate temperature was then reduced to 573 K at which deposition of a Cr buffer layer of 10 nm thickness took place. The Co/Cr superlattice structure of 20 Co/Cr periods was deposited at 423 K to keep interdiffusion at a minimum. The final Co/Cr bilayer of the superstructure was capped with additional 2 nm Cr. The growth rates of Co and Cr were monitored by a calibrated quartz oscillator and were found to be 0.78 nm/min and 0.16 nm/min, respectively. A series of samples has been prepared keeping the nominal thickness of Cr constant while varying the Co thickness.

In this thickness range of a few Co monolayers, the crossover from three to two dimensions sets in, and confinement reduces the Curie temperature[31] from $T_C^\infty(\text{Co})=1388$ K to

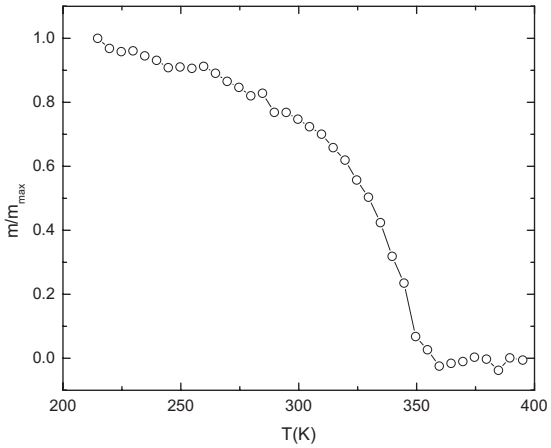

FIG. 2. Normalized magnetic moment $m/m_{\max}$ vs T of noninteracting ultrathin Co films after zero-field cooling and subsequent field heating in $\mu_0 H=5$ mT. The Curie temperature of bulk Co has been reduced by more than 1000 K due to a geometrical confinement of the correlation length perpendicular to the film plane.

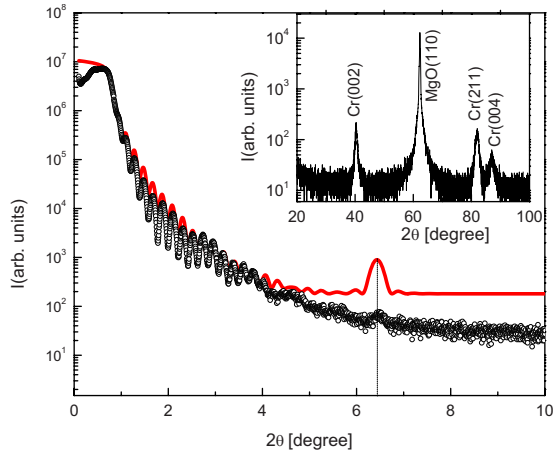

FIG. 3. (Color online) Small-angle x-ray diffraction pattern of a nominal Cr(10 nm)/[Co(0.60 nm)/Cr(0.78 nm)]$_{20}$/Cr(2 nm) superlattice (circles). The line represents a best fit using LEPTOS 2. Indication of a superpeak at $2\theta \approx 6.5°$ is found in the data in agreement with the fit (see dashed vertical line). The inset shows the wide-angle x-ray diffraction pattern indicating a Cr(211) peak from the 10 nm Cr buffer layer, the pronounced MgO (110) of the oriented single crystalline substrate and Cr (00l) peaks from the 2 nm capping layer. The individual ultrathin Co and Cr films appear as superstructure in the small-angle pattern but are not resolved in the wide-angle pattern.

room temperature in accordance with the finite-size scaling,[32]

$$[T_C^{\infty}(\mathrm{Co}) - T_C(n)]/T_C(n) = [(n-n')/n_0]^{-\lambda}. \qquad (18)$$

Here n is the number of deposited monolayers, n_0 is a dimensionless parameter of the order of one to two monolayers while the shift exponent λ is of the order of 1. From finite-size scaling, Eq. (18), one would expect a T_C close to room temperature in the limit of one to two monolayers. Alloying effects at the nonideal Co/Cr interfaces, however, have already a suppressing effect on T_C of Co.[54] Hence, our deposited Co films are about one to two monolayers thicker than the ideal estimate above suggests. Figure 2 shows the normalized temperature dependence of the total magnetic moment, m, of noninteracting ultrathin Co films after zero-field cooling and subsequent field heating in $\mu_0 H=5$ mT. The negligible interplane interaction is reached in the limit of a large Cr spacer thickness of $d_{\mathrm{Cr}}=5$ nm. The Curie temperature of bulk Co has been reduced by more than 1000 K due to a geometrical confinement of the correlation length perpendicular to the film plane.

Figure 3 shows a small-angle x-ray diffraction pattern for the multilayer sample Cr(10 nm)/[Co(0.60 nm)/Cr(0.78 nm)]$_{20}$/Cr(2 nm) as a typical example of our heterostructures. A superstructure peak is visible in the experimental data (circles) at $2\theta=6.5°$ and reproduced by the simulation (solid line) using the LEPTOS-2 software package. A simple estimate with the help of Bragg's law reveals $d \approx \lambda_{\mathrm{Cu}\,K\alpha}/2 \sin 3.25° = 1.4$ nm with the characteristic Cu $K\alpha$ radiation of wavelength $\lambda_{\mathrm{Cu}\,K\alpha}=0.1544$ nm. This thickness represents the period produced by the sum of the Co thickness and the Cr thickness. The large angle x-ray diffraction pattern (Max-B, Rigaku-D) shown in the inset indicates a Cr(211) peak from the 10 nm Cr buffer layer, the pronounced MgO (110) of the oriented single crystalline substrate and Cr (00l) peaks from the 2 nm capping layer. The individual ultrathin Co and Cr films are evidenced as superstructure in the small-angle pattern but are not resolved in the wide-angle pattern (inset Fig. 3).

D. Magnetic properties of the superlattices

A superconducting quantum interference device (SQUID) magnetometer (MPMS-XL, Quantum Design) was used to carry out the magnetic measurements with magnetic fields applied in the plane of the sample. Figure 2 shows the presence of the well-known finite-size effect in a Cr(10 nm)/[Co(0.40 nm)/Cr(5 nm)]$_{20}$/Cr(2 nm) multilayer where the large Cr thickness of 5 nm suppresses to a large extend AF Co-Co interlayer coupling. Hence the FM to PM transition of the ultrathin Co films is observed at a Curie temperature of $T_C(d_{\mathrm{Co}}=0.4\ \mathrm{nm}) \approx 360$ K.

Next we evidence the presence of AF coupling between the Co films. The coupling is mediated by RKKY-like exchange which depends on the Cr layer thickness d_{Cr}. Figure 4 shows a typical hysteresis loop where the zero-field magnetization (remanence) is zero. The upper left inset shows a magnified portion of the hysteresis in the vicinity of $H=0$. Here a tendency toward moment compensation is already visible even when the applied field favors parallel alignment of the Co magnetization. This provides clear evidence for AF coupling. The lower right inset shows a cartoon of the heterostructure indicating the compensation of the Co moments close to $H=0$. Note that magnetic hysteresis gives rise to losses during cyclic magnetization reversal diminishing the magnetocaloric cooling. In the giant magnetocaloric material $Gd_5Ge_2Si_2$ hysteresis has been reduced by 90% through addition of Fe.[14] In magnetic multilayer heterostructures one can achieve control over the magnetic anisotropy which is a

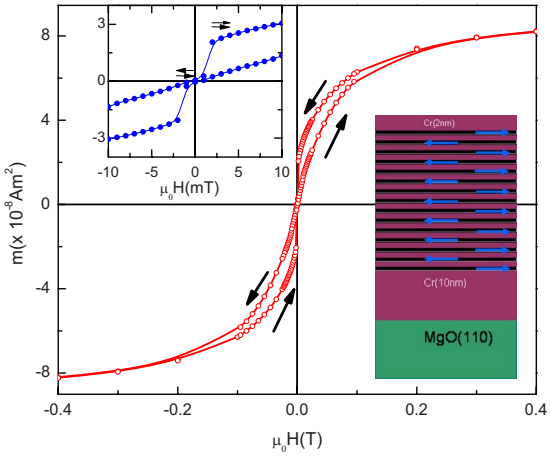

FIG. 4. (Color online) Room-temperature magnetic hysteresis of Cr(10 nm)/[Co(0.80 nm)/Cr(0.75 nm)]$_{10}$/Cr(2 nm). The arrows indicate the directions of field sweeps. The upper left inset shows a detailed view on the hysteresis in the vicinity of zero magnetic field. The compensation of the magnetization in small fields is clearly visible and shows that coupling between the Co films is AF. The arrows in the upper left inset represent the magnetization orientation of neighboring Co films for zero and positive applied magnetic field, respectively. The lower right inset shows a cartoon of the heterostructure and the compensation of the Co moments (arrows) close to $H=0$.

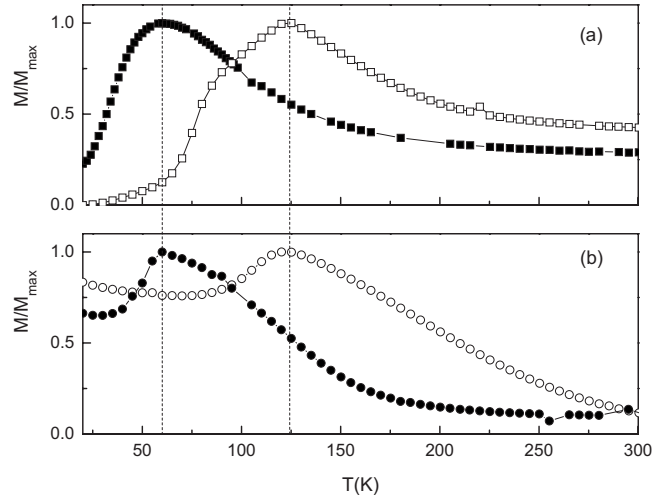

FIG. 5. M/M_{max} vs T of Cr(10 nm)/[Co(d)/Cr(0.75 nm)]$_{20}$/Cr(2 nm) for d_{Co}=0.35 (solid squares) and 0.58 nm (open squares), respectively, measured in an applied magnetic field of 5 mT. Figure 5(b) shows the temperature dependence of Cr(10 nm)/[Co(0.60 nm)/Cr(0.78 nm)]$_{20}$/Cr(2 nm) (solid circles) and Cr(10 nm)/[Co(0.7 nm)/Cr(0.84 nm)]$_{20}$/Cr(2 nm) (open circles) measured in an applied field of 5 mT. The dashed lines are guides for the eyes for the comparison of similar peak positions of different samples.

major factor in determining and potentially reducing hysteresis. The effectiveness of such an approach remains to be investigated in the future.

Next we study the thermodynamics of various Co/Cr superlattices with AF interlayer coupling. In accordance with the mean-field Eq. (11), Fig. 5 suggests that the location of the temperature driven AF to PM transition can be tuned via the intra- and interplane exchange interactions. The intralayer interaction is related to the tunable $T_C(d_{Co})$ of the Co films, the interplane interaction is controlled via the spacing between the Co films.

Figure 5(a) shows M/M_{max} vs T of Cr(10 nm)/[Co(d)/Cr(0.75 nm)]$_{20}$/Cr(2 nm) for d_{Co} =0.35 (solid squares) and 0.58 nm (open squares), measured in an applied magnetic field of 5 mT. The increase in the Co thickness is accompanied by an increase in the T_C of the Co films in accordance with Eq. (18). An increase in T_C can be interpreted as an increase in the effective in-plane exchange constant J_1, even if the microscopic spin-spin exchange is unaffected by changes in the geometrical confinement. At constant Cr thickness (constant J_2), an increasing Co thickness (d_{Co}) therefore enhances the AF transition temperature.

Figure 5(b) allows the comparison of the temperature dependence of Cr(10 nm)/[Co(0.60 nm)/Cr(0.78 nm)]$_{20}$/Cr(2 nm) (solid circles) and Cr(10 nm)/[Co(0.7 nm)/Cr(0.84 nm)]$_{20}$/Cr(2 nm) (open circles) with the results of Fig. 5(a). Again, in accordance with the guiding mean-field arguments of Eq. (11), we find that an increase in d_{Co} from 0.35 to 0.60 nm is compensated by a reduction in the interplane exchange J_2 realized through increased Cr thickness. Similarly an increase in d_{Co} from 0.58 to 0.70 nm (nominally only since x-ray results are inconclusive) implies an increase in the effective J_1 and, hence, enhancement of the AF transition temperature. However, the increase in J_1 is overcompensated by a decrease in J_2. The latter originates from an increase in the Cr thickness from 0.75 to 0.84 nm. Increasing d_{Cr} for d_{Cr} larger than 0.7 nm reduces the AF coupling strength.[33] Note that the decrease in AF coupling strength is also apparent in the incomplete compensation of the low-temperature magnetization of the curves in Fig. 5(b) while the higher AF coupling strength gives rise to almost complete compensation of the low-temperature magnetization [Fig. 5(a)]. A comparison between the curves in Fig. 5(b) is also consistent with the qualitative mean-field Eq. (11) showing that a strong increase in the Co thickness overcompensates for a moderate increase in the Cr thickness and, hence, enhances the transition temperature.

Next we show the magnetization data of Cr(10 nm)/[Co(0.80 nm)/Cr(0.75 nm)]$_{10}$/Cr(2 nm) which can be analyzed in terms of positive MCE near room temperature. Figure 6 shows representative isotherms m vs $\mu_0 H$ for $0 \leq \mu_0 H \leq 7$ T. The complete data set used for the entropy calculation via Maxwell's relation involves the isotherms at $120 \leq T \leq 330$ K in steps of $\Delta T = 10$ K. The inset shows representative field heating and cooling curves, m vs T, at 5 (squares) and 100 mT (triangles). All measurements have been initialized by zero-field cooling. Note that temperature hysteresis is negligible (see arrows for indication of the direction of temperature change).

Figure 7 shows the mass specific entropy change, ΔS, calculated with the help of Maxwell's relation giving rise to Eq. (16) after integration. The latter allows calculating ΔS_m which provides ΔS when normalizing with respect to the magnetically active mass of the sample. The mass is calculated from the sample area of 25 mm^2, the Co and Cr thick-

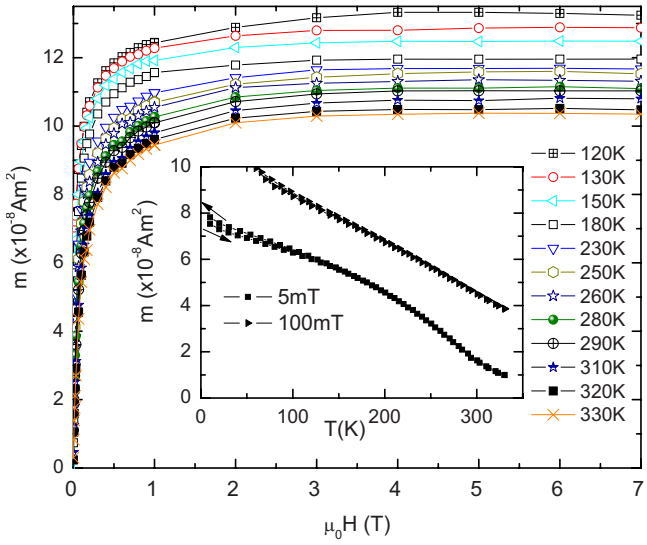

FIG. 6. (Color online) Isotherms m vs $\mu_0 H$ for $0 \leq \mu_0 H \leq 7$ T. The inset shows field heating and cooling m vs T data at 5 mT (squares) and 100 mT (triangles). All curves are initialized by zero-field cooling, and the arrows indicate the direction of the temperature change.

nesses, and their densities. We used the grid of isotherms over the temperature interval $120 \leq T \leq 330$ K to numerically calculate $\frac{\partial m}{\partial T}$ vs $\mu_0 H$ for $0 \leq \mu_0 H \leq 7$ T where $m = VM$. The dotted line shows an extrapolation of $-\Delta S(T)$ toward higher temperature beyond our experimental data. The extrapolation implies that the maximum of the entropy change will be significantly higher than -0.4 J/kg K but located 50 K or more above room temperature. It is apparent from our theoretical considerations in Secs. III A and III B that amplitude and position of the peak of the entropy change can be controlled over a wide range. As discussed throughout the

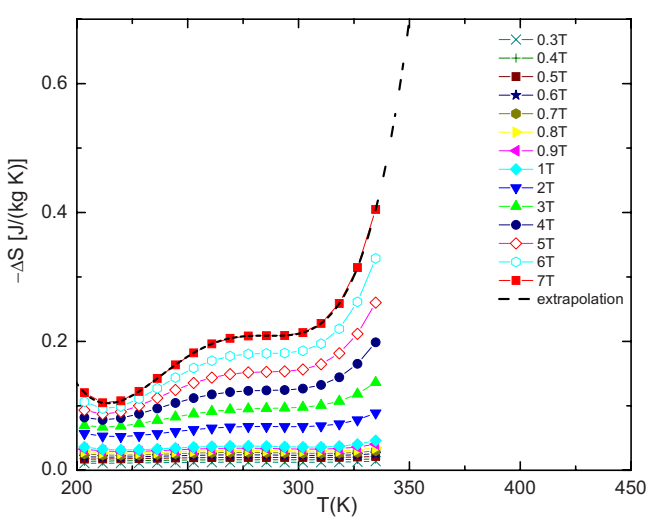

FIG. 7. (Color online) Temperature dependence of the mass specific entropy change ΔS calculated from Eq. (15), using the experimental isotherms in the temperature interval $120 \leq T \leq 330$ K measured in steps of $\Delta T = 10$ K to numerically calculate $\frac{\partial m}{\partial T}$ vs $\mu_0 H$ for $0 \leq \mu_0 H \leq 7$ T. The dotted line shows an extrapolation of $-\Delta S$ vs T toward higher temperature going beyond our experimental data.

paper, the tuning of these essential magnetocaloric properties is achieved through growth controlled modification of J_1 and J_2.

The data shown in Fig. 7 appear encouraging enough to finally estimate the adiabatic temperature change,

$$\Delta T_{\mathrm{ad}} = -T \int_0^{\mu_0 H'} \frac{1}{C} \left(\frac{\partial M}{\partial T} \right)_H d(\mu_0 H). \tag{19}$$

This expression describes the drop in temperature of a sample with positive MCE when removing the applied magnetic field while heat exchange with the surrounding is suppressed. This is an important figure of merit for possible magnetocaloric applications, because it allows, e.g., the calculation of the refrigeration capacity $\mathrm{RC} = \Delta S \times \Delta T$.[9] The phenomenological expression for ΔT_{ad} deviates from the isothermal entropy expression by the additional factor $-T/C(T,H)$ where $C(H,T)$ is the field and temperature dependent heat capacity of the sample. Here, we estimate the latter with the help of the temperature and field-independent high-temperature limit of the heat capacity at constant volume, $C = 3Rn$, where R is the universal gas constant and n is the number of moles of Co and Cr.

With the amount of deposited Co and Cr material $M_{\mathrm{Co}} = 1.67 \times 10^{-9}$ kg and $M_{\mathrm{Cr}} = 3.4 \times 10^{-9}$ kg, we obtain the specific-heat capacity $C \approx 461$ J/kg K. With this and $\Delta S(T = 334\ \mathrm{K}, \mu_0 H = 7\ \mathrm{T}) = -0.4$ J/kg K we estimate

$$\Delta T_{\mathrm{ad}} \approx -\frac{T \Delta S}{C} \approx 0.3\ \mathrm{K}, \tag{20}$$

an appreciable value with significant potential for further improvement.

IV. CONCLUSIONS

The tuning of magnetocaloric properties in nanostructured materials for near room-temperature refrigeration applications has been investigated theoretically and experimentally. Our focus is on artificial antiferromagnetic superlattices with tailored metamagnetic transitions allowing for a negative and a positive magnetocaloric effect below and above the antiferromagnetic transition, respectively. The phase diagram and, hence, the magnetocaloric properties of these metamagnets are largely determined by the in-plane and interplane exchange interactions. We show that a large ratio of intra- to interlayer exchange is favorable for spin-flip transitions with large entropy change. Here the tricritical temperature approaches the Néel temperature which at the same time is near the critical temperature of the ferromagnetic constituent films activating microscopic spin fluctuations for the magnetic entropy change. The maximum field-induced entropy change occurs at about one-half of the tricritical temperature. We realize layered artificial antiferromagnets experimentally with the help of MBE grown Co/Cr superlattices of ultrathin Co and Cr films. SQUID magnetometric studies of the temperature and field dependence of the magnetization are performed for various Co/Cr multilayer systems. The positive magnetocaloric effect is explored for one of these samples with a detailed investigation of the isothermal entropy and

the corresponding adiabatic temperature change.

ACKNOWLEDGMENTS

This research was supported by Teledyne Isco, EPSCoR, NRI, NSF Career Grant No. DMR-0547887 (T.M., S.S., and Ch.B.) and by the DOE (Grant No. DE-F602-04ER46152) and NCMN (R.S. and D.J.S.).

*cbinek2@unlnotes.unl.edu

[1] V. K. Pecharsky and K. A. Gschneidner, Jr., Int. J. Refrigeration **29**, 1239 (2006).
[2] V. K. Pecharsky and K. A. Gschneidner, Jr., J. Magn. Magn. Mater. **200**, 44 (1999).
[3] S. L. Russek and C. Zimm, Int. J. Refrigeration **29**, 1366 (2006).
[4] K. A. Gschneidner, Jr., V. K. Pecharsky, and A. O. Tsokol, Rep. Prog. Phys. **68**, 1479 (2005).
[5] C. Zimm, A. Boeder, J. Chell, A. Sternberg, A. Fujita, S. Fujieda, and K. Fukamichi, Int. J. Refrigeration **29**, 1302 (2006).
[6] http://en.wikipedia.org/wiki/Magnetocaloric_effect and references there in.
[7] X. Bohigas, E. Molins, A. Roig, J. Tejada, and X. X. Zhang, IEEE Trans. Magn. **36**, 538 (2000).
[8] L. Chen and Z. Yan, J. Appl. Phys. **75**, 1249 (1994).
[9] M. E. Wood and W. H. Potter, Cryogenics **25**, 667 (1985).
[10] D. J. Sellmyer and R. Skomski, *Advanced Magnetic Nanostructures* (Springer, New York, 2006).
[11] R. Skomski and J. M. Coey, *Permanent Magnetism* (Institut of Physics, Bristol, 1999).
[12] H. Wada and Y. Tanabe, Appl. Phys. Lett. **79**, 3302 (2001).
[13] V. K. Pecharsky and K. A. Gschneidner, Jr., Phys. Rev. Lett. **78**, 4494 (1997).
[14] V. Provenzano, A. J. Shapiro, and R. D. Shull, Nature (London) **429**, 853 (2004).
[15] T. Krenke, E. Duman, M. Acet, E. F. Wassermann, X. Moya, L. Manosa, and A. Planes, Nature Mater. **4**, 450 (2005).
[16] O. Tegus, E. Brueck, K. H. J. Buschow, and F. R. de Boer, Nature (London) **415**, 150 (2002).
[17] V. K. Pecharsky, A. P. Holm, K. A. Gschneidner, Jr., and R. Rink, Phys. Rev. Lett. **91**, 197204 (2003).
[18] K. A. Gschneidner, Jr. and V. K. Pecharsky, Annu. Rev. Mater. Sci. **30**, 387 (2000).
[19] M. D. Kuz'min, Appl. Phys. Lett. **90**, 251916 (2007).
[20] C. S. Aleves, S. Gama, A. de A. Coelho, E. J. R. Plaza, A. M. G. Carvalho, L. P. Cardoso, and A. C. Persiano, Mater. Res. **7**, 535 (2004).
[21] A. de Campos, D. L. Rocco, A. Magnus, G. Carvalho, L. Caron, A. A. Coelho, S. Gama, L. M. da Silva, F. C. G. Gandra, A. O. dos Santos, L. P. Cardoso, P. J. von Ranke, and N. A. de Oliveira, Nature Mater. **5**, 802 (2006).
[22] S. Fujieda, A. Fujita, and K. Fukamichi, Appl. Phys. Lett. **81**, 1276 (2002).
[23] S. B. Roy, P. Chaddah, V. K. Pecharsky, and K. A. Gschneidner, Jr., Acta Mater. **56**, 5895 (2008).
[24] A. Giguere, M. Foldeaki, W. Schnelle, and E. Gmelin, J. Phys.: Condens. Matter **11**, 6969 (1999).
[25] T. Samanta, I. Das, and S. Banerjee, Appl. Phys. Lett. **91**, 082511 (2007).
[26] P. Chen and Y. W. Du, J. Phys. Soc. Jpn. **70**, 1080 (2001).
[27] N. K. Sun, S. Ma, Q. Zhang, J. Du, and Z. D. Zhang, Appl. Phys. Lett. **91**, 112503 (2007).
[28] R. Skomski, Ch. Binek, T. Mukherjee, S. Sahoo, and D. J. Sellmyer, J. Appl. Phys. **103**, 07B329 (2008).
[29] A. Cho, J. Vac. Sci. Technol. **8**, S31 (1971).
[30] M. Farle, K. Baberschke, U. Stetter, A. Aspelmeier, and F. Gerhardter, Phys. Rev. B **47**, 11571 (1993).
[31] F. Huang, M. T. Kief, G. J. Mankey, and R. F. Willis, Phys. Rev. B **49**, 3962 (1994).
[32] F. Huang, M. T. Kief, G. J. Mankey, and R. F. Willis, J. Appl. Phys. **73**, 6760 (1993).
[33] G. Gubbiotti, G. Carlotti, L. Giovannini, and L. Smardz, Phys. Status Solidi A **196**, 16 (2003).
[34] O. Hellwig, A. Berger, and E. E. Fullerton, Phys. Rev. Lett. **91**, 197203 (2003).
[35] T. Hauet, C. M. Guenther, O. Hovorka, A. Berger, M. Y. Im, P. Fischer, T. Eimueller, and O. Hellwig, Appl. Phys. Lett. **93**, 042505 (2008).
[36] J. U. Thiele, T. Hauet, and O. Hellwig, Appl. Phys. Lett. **92**, 242502 (2008).
[37] E. J. R. Plaza and J. C. P. Campoy, J. Magn. Magn. Mater. **321**, 446 (2009).
[38] H. Wende, C. Sorg, M. Bernien, A. Scherz, P. J. Jensen, N. Ponpandian, and K. Baberschke, Phys. Status Solidi B **243**, 165 (2006).
[39] P. Grünberg, R. Schreiber, Y. Pang, M. B. Brodsky, and H. Sowers, Phys. Rev. Lett. **57**, 2442 (1986).
[40] H. Zabel, J. Phys.: Condens. Matter **11**, 9303 (1999).
[41] P. Bruno, Phys. Rev. B **52**, 411 (1995).
[42] E. Fawcett, Rev. Mod. Phys. **60**, 209 (1988).
[43] J. M. Kincaid and E. G. D. Cohen, Phys. Rep., Phys. Lett. **22**, 57 (1975).
[44] A. F. S. Moreira, W. Figueiredo, and V. B. Henriques, Eur. Phys. J. B **27**, 153 (2002).
[45] W. Selke, Z. Phys. B: Condens. Matter **101**, 145 (1996).
[46] Ch. Binek, *Ising-type Antiferromagnets: Model Systems in Statistical Physics and in the Magnetism of Exchange Bias* (Springer, Berlin, 2003).
[47] R. B. Griffiths, Phys. Rev. Lett. **24**, 1479 (1970).
[48] I. S. Jacobs and P. E. Lawrence, Phys. Rev. **164**, 866 (1967).
[49] R. J. Birgeneau, W. B. Yelon, E. Cohen, and J. Makovsky, Phys. Rev. B **5**, 2607 (1972).
[50] L. J. De Jongh and A. R. Miedema, Adv. Phys. **23**, 1 (1974).
[51] Ch. Binek, Phys. Rev. Lett. **81**, 5644 (1998).
[52] J. Skalyo, Jr., A. F. Cohen, S. A. Friedberg, and R. B. Griffiths, Phys. Rev. **164**, 705 (1967).
[53] H. Oesterreicher and F. T. Parker, J. Appl. Phys. **55**, 4334 (1984).
[54] T. P. A. Hase, I. Pape, B. K. Tanner, S. M. Thompson, S. M. Jordan, and J. J. Freijo, Adv. X-Ray Anal. **40**, 142 (1996).